Proceedings

Unscented Kalman Filter empowered by Bayesian Model Evidence for System Identification in Structural Dynamics †

Luca Rosafalco [1,2,*], Saeed Eftekhar Azam [2], Andrea Manzoni [3], Alberto Corigliano [1] and Stefano Mariani [1]

[1] Dipartimento di Ingegneria Civile ed Ambientale, Politecnico di Milano, Piazza L. da Vinci 32, 20133 Milano, Italy; alberto.corigliano@polimi.it (A.C.); stefano.mariani@polimi.it (S.M.)
[2] Civil and Environmental Engineering, University of New Hampshire, 33 Academic Way, 03824, Durham, NH, USA; Saeed.EftekharAzam@unh.edu (S.E.); stefano.mariani@polimi.it (S.M.)
[3] MOX, Dipartimento di Matematica, Politecnico di Milano, Piazza L. da Vinci 32, 20133 Milano, Italy; andrea1.manzoni@polimi.it
* Correspondence: luca.rosafalco@polimi.it
† Presented at the First International Online Conference on Algorithms, 27 September–10 October 2021; Available online: https://ioca2021.sciforum.net/.

Abstract: System identification is often limited to parameter identification, while model uncertainties are disregarded or accounted for by a fictitious process noise. However, modelling assumptions may have a large impact on system identification. For this reason, we propose to use an Unscented Kalman Filter (UKF) empowered with online Bayesian model evidence computation for the sake of system identification and model selection. This approach employs more than one model to track the state of the system and associates to each model a plausibility measure, updated whenever new measurements are available. The filter outcomes obtained for different models are then compared and a quantitative confidence value is associated to each of them. Only the system identification outcomes related to the model with the highest plausibility are considered. While the coupling of Extended Kalman Filters (EKFs) and Bayesian model evidence was already addressed, we modified the approach to exploit the most striking features of the UKF, namely the ease of implementation and the higher-order accuracy in the description of the evolution of the state mean and variance. A challenging identification problem related to structural dynamics is discussed to show the effectiveness of the proposed methodology.

Keywords: System identification; unscented Kalman filter; model evidence calculation; model class selection; structural dynamics.

1. Introduction

Kalman Filters (KFs) are well known tools for system identification. They work by applying a predictor phase, in which a suitable model is needed to predict the evolution of a dynamic system, and a correction phase, in which corrections to the prediction are applied by recursively processing system measurements [1].

In civil and mechanical engineering, different model classes, consisting of different parametrizations of the structure to be identified, can be formulated. They are built upon different levels of complexity in the description of the system mechanics, and uncertainty in the formulation of the modelling assumptions. Emphasis is usually placed on improving the quality of the parameter estimate, especially whenever non linear dynamic systems are handled. With this goal, KF extensions such as the Extended Kalman Filter (EKF) or the Unscented Kalman Filter (UKF) have been introduced. On the contrary, model uncertainties are often disregarded or accounted for by a fictious process noise. In this work, we propose a way to tackle this aspect by calculating a quantitative estimate, referred to as model evidence, measuring how much the model employed by the KF is plausible with respect to other possible parametrizations. While a similar estimate was discussed in [2] for the EKF, here we develop a model evidence formula

Published: date

suited for the UKF to exploit its ease of implementation and higher-order accuracy in the description of the evolution of the state mean and variance.

The reminder of the contribution is organized as follows. In Sec. 2, first the governing equations of a mechanical elasto-dynamic system are discussed; second, the related algorithm showing the application of the UKF for parameter estimation is reported; finally, the equations allowing for recursive model evidence calculation are presented. In Sec. 3, a case study featuring a shear building excited by a real ground acceleration is discussed, showing how parameter identification outcomes are affected by different structural parametrizations and how model evidence can be used for the sake of model selection a posteriori. Conclusions are finally discussed in Sec. 4.

2. Methodology

2.1. Elasto-dynamic problem

We focus on situations where the system dynamics is described by the Finite Element (FE) discretised version of a general elasto-dynamic problem. At time t_{k+1}, it reads:

$$\mathbf{M}\ddot{\mathbf{q}}_{k+1} + \mathbf{C}\dot{\mathbf{q}}_{k+1} + \mathbf{K}\mathbf{q}_{k+1} = \mathbf{f}_{k+1}, \quad k = 0, \dots, n_{t-1} \tag{1}$$

$\mathbf{M}$, $\mathbf{C}$, $\mathbf{K}$ are the mass, damping and stiffness matrices, respectively; $\mathbf{q}, \dot{\mathbf{q}}, \ddot{\mathbf{q}} \in \mathbb{R}^{n\times 1}$ are the nodal displacements, velocities, accelerations; $\mathbf{f}_{k+1} \in \mathbb{R}^{n\times 1}$ is the external force vector, assumed to be known.

Eq. (1) is integrated in time by using the α-method [3], ruled by the parameters α_m, α_f, β. At each time step, the displacement field $\mathbf{q}_{k+1}$ is obtained by solving

$$\mathbf{K}^*_{k+1}\mathbf{q}_{k+1} = \mathbf{f}^*_{k+1}(\mathbf{q}_k, \dot{\mathbf{q}}_k, \ddot{\mathbf{q}}_k). \tag{2}$$

The modified matrix $\mathbf{K}^*$ and the right hand side vector $\mathbf{f}^*_{k+1}$ are computed as

$$\mathbf{K}^*_{k+1} = \frac{1-\alpha_m}{\beta\Delta t^2}\mathbf{M} + \frac{\gamma\left(1-\alpha_f\right)}{\beta\Delta t}\mathbf{C} + \left(1-\alpha_f\right)\mathbf{K}, \tag{3}$$

$$\begin{aligned}\mathbf{f}^*_{k+1}(\mathbf{q}_k, \dot{\mathbf{q}}_k, \ddot{\mathbf{q}}_k) = \mathbf{f}_{k+1-\alpha_f} + \left(\frac{1-\alpha_m}{\beta\Delta t^2}(\mathbf{q}_k + \Delta t\dot{\mathbf{q}}_k) + \frac{1+\alpha_m-2\beta}{2\beta}\ddot{\mathbf{q}}_k\right)\mathbf{M} + \\ \left(\frac{\gamma\left(1-\alpha_f\right)}{\beta\Delta t}\mathbf{q}_k - \frac{\beta-\gamma\left(1-\alpha_f\right)}{\beta}\dot{\mathbf{q}}_k - \left(1-\frac{\gamma}{2\beta}\right)\left(1-\alpha_f\right)\Delta t\ddot{\mathbf{q}}_k\right)\mathbf{C} - \alpha_f\mathbf{K},\end{aligned} \tag{4}$$

where $\Delta t = t_{k+1} - t_k$, $t_{k+1-\alpha_f} = \left(1-\alpha_f\right)t_{k+1} + \alpha_f t_k$, $\mathbf{f}_{k+1-\alpha_f} = \mathbf{f}\left(t_{k+1-\alpha_f}\right)$.

Moreover, the mechanical system is assumed to be only partially observed. Accordingly, a boolean matrix $\mathbf{H} \in \mathbb{R}^{n_o\times 3n}$ establishes the connection between the n_o observed quantities $\hat{\mathbf{y}}_{k+1} \in \mathbb{R}^{n_o}$ and the kinematic fields, as follows:

$$\hat{\mathbf{y}}_{k+1} = \mathbf{H}[\mathbf{q}_{k+1}, \dot{\mathbf{q}}_{k+1}, \ddot{\mathbf{q}}_{k+1}]^T. \tag{5}$$

2.2. Unscented Kalman Filter for parameter estimation

The goal of filtering is to estimate the unknown parameters $\boldsymbol{\theta} \in \mathbb{R}^{n_p\times 1}$ ruling the mechanical response of the structure to be identified, where typically $\mathbf{C} = \mathbf{C}(\boldsymbol{\theta})$ and $\mathbf{K} = \mathbf{K}(\boldsymbol{\theta})$. In [1,4], Kalman filtering techniques were successfully applied, even in presence of non-linearities due to damage evolution in the observed system, by solving a dual estimation problem, and thereby adopting as state variables the model displacements and the unknown parameters governing the response of the mechanical domain. However, treating FE solutions characterized by a large number n of degrees of freedom (dofs) may result in an excessive computational burden when dealing with dual

estimation. A possible solution constists of obtaining a Reduced Order Model (ROM) representation of the mechanical domain and from adopting as state variables, instead of the nodal kinematics, the ROM dofs [5,6]. This strategy has been explored in [7]. Here, we consider just $\boldsymbol{\theta}$ as state variable to avoid the computational burden connected to the combined use of the UKF and dofs tracking when large FE models are addressed, despite the good performance usually guaranteed by state tracking [1,8]. The following state-space representation is used

$$\boldsymbol{\theta}_{k+1} = \boldsymbol{\theta}_k + \mathbf{w}_k \tag{6a}$$

$$\mathbf{y}_{k+1} = \hat{\mathbf{y}}_{k+1} + \mathbf{v}_{k+1} \tag{6b}$$

where the $\boldsymbol{\theta}$ is driven by a random walk ruled by $\mathbf{w}_k \in \mathbb{R}^{n_p \times 1}$, modelled as a white process noise $\mathbf{w}_k \sim \mathcal{N}(\mathbf{0}, \mathbf{Q})$, and the FE predicted output $\hat{\mathbf{y}}_{k+1}$ is related to the actual response of the structure by adding a measurement noise $\mathbf{v}_{k+1} \in \mathbb{R}^{n_y \times 1}$, modelled as white $\mathbf{v}_{k+1} \sim \mathcal{N}(\mathbf{0}, \mathbf{R})$. The matrices $\mathbf{Q}$ and $\mathbf{R}$ are symmetric and positive defined. The time variation of $\boldsymbol{\theta}$, introduced by the random walk formulation, is fictitious.

KFs attempts to propagate the mean and the covariance of the state variable vector through the state-space and the measurement update equations. Instead of propagating the probability density functions associated to the state variables, it is indeed preferable to deterministically propagate a vector, and to compute the state variable mean and covariance in a second time, especially when the state-space and the measurement update equations are non linear. The UKF is based on this idea. The propagated vector collects a set of Sigma Points (SPs) $\boldsymbol{\vartheta}_k^i$, $i = 1, \ldots, (2n_\theta + 1)$, distributed such that the mean and covariance of these points match those of the state variables. A scaled version of the UKF is used by setting the parameters α_{SP}, κ_{SP} and β_{SP}, as detailed in [9], to avoid sampling non-local effects that would spoil the state variable mean and covariance reconstruction [10]. In the predictor phase, this vector is propagated from the k-th to the $k+1$-th time step through the state-space equations. In the corrector phase, the estimated output covariance $\hat{\mathbf{P}}^{yy}_{k+1|k}$ and the estimated cross covariance $\hat{\mathbf{P}}^{\theta y}_{k+1|k}$ are used to compute the Kalman gain $\mathbf{G}_{k+1}$ needed to correct the propagated mean $\hat{\boldsymbol{\theta}}_{k+1|k}$ and covariance $\hat{\mathbf{P}}^{\theta\theta}_{k+1|k}$ on the basis of the collected measurements $\mathbf{y}_{k+1}$. The full expression of these quantities and the application of the UKF are detailed in Algorithm 1, adapted from [11].

2.3. Model evidence computation for Unscented Kalman Filter

System identification is usually limited to select a particular parametric model $\mathcal{M}$ of the underlying structural system, estimating the corresponding unknown parameters $\boldsymbol{\theta}$. However, the use of either excessively simplified or too complex models may have a detrimental effect on the possibility to track the system state: oversimplified models may underestimate the effect of a physical process taking place; on the other hand, complex models may lead to good data fitting although possibly yielding to poor predictions. In the latter case, the model overfits the incoming data. In [2], an online model class selection strategy was proposed in the framework of EKFs parameter estimates. Here, a similar approach has been adopted for simultaneous parametric estimate and model class selection exploiting the UKF. Adopting a number n_m of possible model classes, the model evidence (or plausibility) consisting of the probability $p(\mathcal{M}^m_{k+1}) \in (0, 1)$ has been computed for each model class $\mathcal{M}^m$, with $m = 1, \ldots, n_m$ at each time step t_{k+1}. The sum of the n_m model evidences is equal to the unity. To derive the expression of $p(\mathcal{M}^m_{k+1})$, first the Bayes theorem has been used, giving

$$p(\mathcal{M}^m_{k+1}) = \frac{p(\mathbf{y}_{k+1}|\mathcal{M}^m_k)\, p(\mathcal{M}^m_k)}{\sum_{l=1}^{n_m} p(\mathbf{y}_{k+1}|\mathcal{M}^l_k)\, p(\mathcal{M}^l_k)}\,, \tag{7}$$

where $p(\mathbf{y}_{k+1}|\mathcal{M}_k^m)$, called conditional evidence, represents the contribution of the measurement at t_{k+1} to the plausibility of the m-th model class.

Second, we have extended the procedure explained in [2] from the EKF to the UKF. As a result, at the end of the corrector phase (after step 15 of Algorithm 1), the following expression for the conditional evidence applies

$$\begin{aligned} p(\mathbf{y}_{k+1}|\hat{\boldsymbol{\theta}}, \mathcal{M}_k^m) \approx (2\pi)^{-\frac{n_\theta}{2}} \left[\det\left(\hat{\mathbf{P}}_{k+1|k+1}^{\theta\theta}\left(\hat{\mathbf{P}}_{k+1|k}^{\theta\theta}\right)^{-1}\right)\right]^{\frac{1}{2}} \left[\det\left(\hat{\mathbf{P}}_{k+1|k}^{yy\,-1}\right)\right]^{\frac{1}{2}} \\ \times \exp\left[-\frac{1}{2}\left(\hat{\boldsymbol{\theta}}_{k+1|k+1} - \hat{\boldsymbol{\theta}}_{k+1|k}\right)^T \left(\hat{\mathbf{P}}_{k+1|k}^{\theta\theta}\right)^{-1}\left(\hat{\boldsymbol{\theta}}_{k+1|k+1} - \hat{\boldsymbol{\theta}}_{k+1|k}\right)\right. \\ \left. -\frac{1}{2}\left(\mathbf{y}_{1:k+1} - \hat{\mathbf{y}}_{1:k+1|k}\right)^T \left(\hat{\mathbf{P}}_{k+1|k}^{yy}\right)^{-1}\left(\mathbf{y}_{1:k+1} - \hat{\mathbf{y}}_{1:k+1|k}\right)\right], \end{aligned} \tag{8}$$

where $\det(\cdot)$ calculates the determinant of the input matrix. The reported expression approximates $p(\mathbf{y}_{k+1}|\hat{\boldsymbol{\theta}}, \mathcal{M}_k^m)$ due to the use of the Laplace's asymptotic expansion [2].

Algorithm 1 UKF for parameter estimation, linear elastic case.

1: for $k = 0, \ldots, n_t$ ▷ loop over the time steps

Predictor phase

2: Assume $\hat{\boldsymbol{\theta}}_{k+1|k} = \hat{\boldsymbol{\theta}}_{k|k}$, according to Eq. 6a ▷ prior estimate of the state variables
3: Assume $\hat{\boldsymbol{P}}_{k+1|k}^{\theta\theta} = \hat{\mathbf{P}}_{k|k}^{\theta\theta} + \mathbf{Q}$ ▷ prior covariance of the state variable estimate
4: Generate $\boldsymbol{\vartheta}_{k+1}^i$, $i = 1, \ldots, (2n_\theta + 1)$ using $\hat{\boldsymbol{\theta}}_{k+1|k}$, $\hat{\mathbf{P}}_{k+1|k}^{\theta\theta}$ as in [9] ▷ SPs
5: Compute $\mathbf{q}_{k+1}^i = \left(\mathbf{K}_{k+1}^{*i}\left(\boldsymbol{\vartheta}_{k+1}^i\right)\right)^{-1} \mathbf{f}_{k+1}^i\left(\mathbf{q}_k, \dot{\mathbf{q}}_k, \ddot{\mathbf{q}}_k, \boldsymbol{\vartheta}_{k+1}^i\right)$ ▷ displacement field for each SP
6: Compute $\dot{\mathbf{q}}_{k+1}^i, \ddot{\mathbf{q}}_{k+1}^i$ ▷ velocity and acceleration fields for each SP
7: Compute $\mathfrak{y}_{k+1}^i = \mathbf{H}\left[\mathbf{q}_{k+1}^i, \dot{\mathbf{q}}_{k+1}^i, \ddot{\mathbf{q}}_{k+1}^i\right]^T$ ▷ system observation for each SP
8: Compute $\hat{\mathbf{y}}_{k+1|k} = \sum_{i=1}^{2n_\theta+1} w_m^i \mathfrak{y}_{k+1}^i$ ▷ predicted output

Corrector phase

9: Compute $\hat{\mathbf{P}}_{k+1|k}^{yy} = \sum_{i=1}^{2n_\theta+1} w_c^i \left[\mathfrak{y}_{k+1}^i - \hat{\mathbf{y}}_{k+1|k}\right]\left[\mathfrak{y}_{k+1}^i - \hat{\mathbf{y}}_{k+1|k}\right]^T + \mathbf{R}$ ▷ estimated output covariance
10: Compute $\hat{\mathbf{P}}_{k+1|k}^{\theta y} = \sum_{i=1}^{2n_\theta+1} w_c^i \left[\boldsymbol{\vartheta}_{k+1}^i - \hat{\boldsymbol{\theta}}_{k+1|k}\right]\left[\mathfrak{y}_{1:k+1}^i - \hat{\mathbf{y}}_{1:k+1|k}\right]^T$ ▷ estimated cross covariance
11: Compute $\mathbf{G}_{k+1} = \hat{\mathbf{P}}_{k+1|k}^{\theta y}\left(\hat{\mathbf{P}}_{k+1|k}^{yy}\right)^{-1}$ ▷ Kalman gain
12: Update the prior estimate $\hat{\boldsymbol{\theta}}_{k+1|k+1} = \hat{\boldsymbol{\theta}}_{k+1|k} + \mathbf{G}_{k+1}\left(\mathbf{y}_{k+1} - \hat{\mathbf{y}}_{k+1|k}\right)$ ▷ posterior estimate of the state variables
13: Update the prior estimate $\hat{\mathbf{P}}_{k+1|k+1}^{\theta\theta} = \hat{\mathbf{P}}_{k+1|k}^{\theta\theta} - \mathbf{G}_{k+1}\hat{\mathbf{P}}_{k+1|k}^{yy}\mathbf{G}_{k+1}^T$ ▷ posterior covariance of the state variable estimate
14: Compute $\mathbf{q}_{k+1} = \left(\mathbf{K}_{k+1}^*\left(\hat{\boldsymbol{\theta}}_{k+1|k+1}\right)\right)^{-1} \mathbf{rhs}_{k+1}\left(\mathbf{q}_k, \dot{\mathbf{q}}_k, \ddot{\mathbf{q}}_k, \hat{\boldsymbol{\theta}}_{k+1|k+1}\right)$ ▷ displacement field
15: Compute $\dot{\mathbf{q}}_{k+1}, \ddot{\mathbf{q}}_{k+1}$ ▷ velocity and acceleration fields
16: end for

3. Results and Discussion

As a numerical case study, we have studied how to determine the interstory stiffness and damping of the two dof shear building model ($n = 2$) reported in Fig. 1. The

mechanical properties of the building have been adimensionalized to ease the UKF tuning by setting the matrices in Eq. (1) equal to

$$\mathbf{M} = \begin{bmatrix} 2 & 0 \\ 0 & 2 \end{bmatrix}, \qquad \mathbf{C} = \begin{bmatrix} 0.2 & -0.1 \\ -0.1 & 0.1 \end{bmatrix}, \qquad \mathbf{K} = \begin{bmatrix} 2 & -1 \\ -1 & 1 \end{bmatrix}.$$

The building has been excited by the ground acceleration $\mathbf{a}_0$ reported in Fig. 2, lasting 60 s. The response of the building has been monitored by recording the floor acceleration $\mathbf{y} = [y_1, y_2]^T$ with a sampling frequency of 50 Hz, for a total of $n_t = 3000$ samples. A white noise, featuring a standard deviation of $5 \cdot 10^{-3}$, has been added to y_1 and to y_2 to mimic the signal perturbation affecting micro-electro mechanical accelerometers [12].

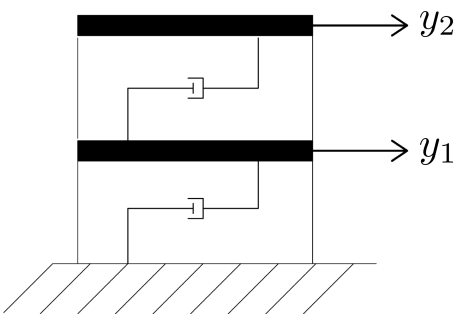

Figure 1. Two dofs shear model. Acceleration monitoring.

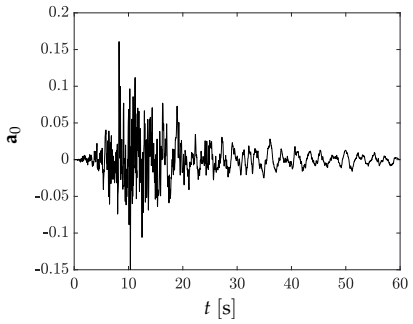

Figure 2. Ground acceleration.

The acceleration recordings coming from this reference building have been used as measurements in the corrector phase of the filtering procedure (step 9 and 10 of Algorithm 1). Three model classes, $\mathcal{M}^1$, $\mathcal{M}^2$, $\mathcal{M}^3$, featuring different structural parametrization, have been considered, as shown in the following

$$\mathbf{C}^1 = \begin{bmatrix} 0.12 & -0.06 \\ -0.06 & 0.06 \end{bmatrix}, \qquad \mathbf{K}^1\left(\theta_1^1\right) = \theta_1^1 \begin{bmatrix} 2 & -1 \\ -1 & 1 \end{bmatrix}$$

$$\mathbf{C}^2\left(\theta_2^2\right) = \theta_2^2 \begin{bmatrix} 0.2 & -0.1 \\ -0.1 & 0.1 \end{bmatrix}, \qquad \mathbf{K}^2\left(\theta_1^2\right) = \theta_1^2 \begin{bmatrix} 2 & -1 \\ -1 & 1 \end{bmatrix}$$

$$\mathbf{C}^3\left(\theta_3^3\right) = \theta_3^3 \begin{bmatrix} 0.2 & -0.1 \\ -0.1 & 0.1 \end{bmatrix}, \qquad \mathbf{K}^3\left(\theta_1^3, \theta_2^3\right) = \begin{bmatrix} \theta_1^3\theta_2^3 & -\theta_2^3 \\ -\theta_2^3 & \theta_2^3 \end{bmatrix}.$$

Model class $\mathcal{M}^1$ is governed by the parameter θ_1^1 ruling the inter storey stiffness of both floors (for this reason, θ_1^1 is factored out from $\mathbf{K}^1$); $\mathcal{M}^2$ is governed by $\boldsymbol{\theta}^2 = \left[\theta_1^2, \theta_2^2\right]^T$, ruling, respectively, the inter storey stiffness and damping of both floors; $\mathcal{M}^3$ is governed by $\boldsymbol{\theta}^3 = \left[\theta_1^3, \theta_2^3, \theta_3^3\right]^T$, where θ_1^3 and θ_2^3 rules the first and second floor inter storey stiffness, θ_3^3 rules the damping associated to both floors. Comparing these parametrizations with the reference model, it is clear that $\mathcal{M}^1$ is under parametrizing the mechanical system, not associating any parameter to the damping properties of the structures and suffering a model bias, being $\mathbf{C}^1 = 0.6\ \mathbf{C}$; $\mathcal{M}^3$ is over parametrizing the stiffness matrix; $\mathcal{M}^2$ is performing a correct parametrization of the structural response, and it is therefore expected to allow for the best estimate of the system mechanical properties. For all model classes, the initial guess of the relevant parameters have underestimated of 40% the parameter values ruling the reference structure.

KF tuning is usually problem-dependent and is performed through a trial-and-error procedure. In this case, we have set the SP scaling parameters to $\alpha_{SP} = 10^{-3}$, $\kappa_{SP} = 0$, $\beta_{SP} = 2$; the measurement noise covariance to $\mathbf{R} = 4 \cdot 10^{-4}\ \mathbf{I}_2$, where $\mathbf{I}_2 \in \mathbb{R}^{2\times 2}$ is the identity matrix; the process noise covariance to $\mathbf{Q} = 10^{-8}\ \mathbf{I}_{n_p}$, with $\mathbf{I}_{n_p} \in \mathbb{R}^{n_p \times n_p}$; the

initial parameter covariance to $\hat{\mathbf{P}}_0^{\theta\theta} = 0.25\ \mathbf{I}_{n_p}$. The value of n_p depends on the number of parameters employed by each model ($n_p = 1$ for $\mathcal{M}^1$, $n_p = 2$ for $\mathcal{M}^2$, $n_p = 3$ for $\mathcal{M}^3$).

In Fig. 3 the predicted output of $\mathcal{M}^1$, computed according to step 8 of Algorithm 1, is reported against the floor acceleration measurements, showing the filter capacity of tracking the shear building accelerations despite the presence of noise. A small discrepancy between the reference model and the predicted output is observable only magnifying the curves. The predicted output of $\mathcal{M}^2$ and $\mathcal{M}^3$, not reported for lack of space, exhibit an even smaller discrepancy.

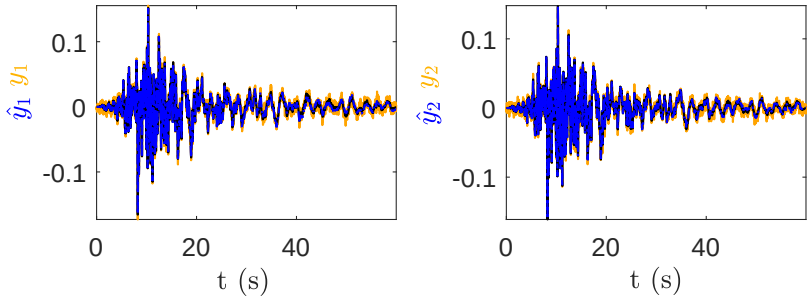

Figure 3. $\mathcal{M}^1$ predicted outputs (dot dashed blue line) is reported against the noise corrupted reference model recordings (orange line). The left figure refers to the first floor, the right figure to the second floor. Black lines depict the reference model acceleration when not corrupted by noise.

The filter capacity of tracking the system output is expected to greatly help parameter identification. In Figs. 4-6 the time evolution of the parameters employed by $\mathcal{M}^1$, $\mathcal{M}^2$ and $\mathcal{M}^3$ are reported, respectively. Black color is used for parameters involved in the expression of the structural stiffness; orange color when related to the structural damping. The plots report both the parameter posterior estimates and the confidence intervals of these estimates. Looking at the confidence intervals, stiffness related parameters seem to assume negative values during the first part of the analyses. This is due to to the initial choice of $\hat{\mathbf{P}}_0^{\theta\theta} = 0.25\ \mathbf{I}_{n_p}$. However, positive values have been always associated with the inter-storey stiffness thank to the use of the scaled version of the UKF. A similar reasoning applies to damping related parameters.

Looking at Fig. 4, the UKF has been unable to provide a correct estimate for θ_1^1, despite the uncertainty reduction linked to the narrowing of the confidence interval. Even the stiffness related parameters θ_1^3 and θ_2^3 of $\mathcal{M}^2$, depicted in Fig. 6, seem not able to converge to the desired value. On the contrary, coming to $\mathcal{M}^2$, θ_1^2 has been correctly identified with small uncertainty, as shown in Fig. 5. These results were somehow how expected due to the under parametrization of the mechanical system operated by $\mathcal{M}^1$, and the over parametrization of the mechanical system exhibited by $\mathcal{M}^3$, while $\mathcal{M}^2$ embodies the correct description of the reference model.

Model class $\mathcal{M}^3$ has been unable to provide any idea of the damping properties, ending up pushing θ_3^3 to 0. Model class $\mathcal{M}^2$ has provided a better estimate, still quite poor, over estimating of 40% the damping related parameter θ_2^2. These difficulties have been due to the relevance of damping in the identification of continuously excited structure, discussed in [4].

From the results reported above, $\mathcal{M}^2$ seems to lead to the best system identification, however we reached this conclusion by knowing the mechanical properties of the reference system. It would have been very hard, if not impossible to judge model plausibility just looking at the predicted outputs. Indeed, as shown in Fig. 3, the UKF has been able to reproduce the monitoring system outcome even when $\mathcal{M}^1$ has been employed. For this reason, model evidence computation, whose outcome is reported in Fig. 7, is extremely relevant to understand which model can be trusted the most.

At the beginning of the identification procedure, equal plausibility has been associated to the three models. Their values have been recursively updated as soon as new

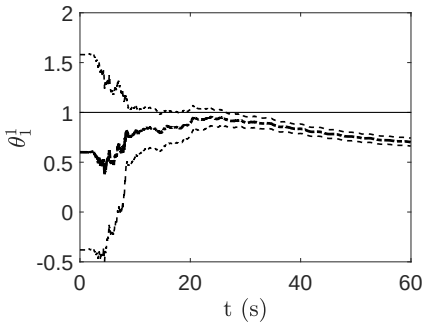

Figure 4. Model class $\mathcal{M}^1$, time evolution of θ_1^1. The thicker dotted line reports the posterior estimate, the thinner dotted lines the 99% confidence interval of the estimate, determined using the posterior covariance. The continuous line reports the parameter value assumed by the reference model.

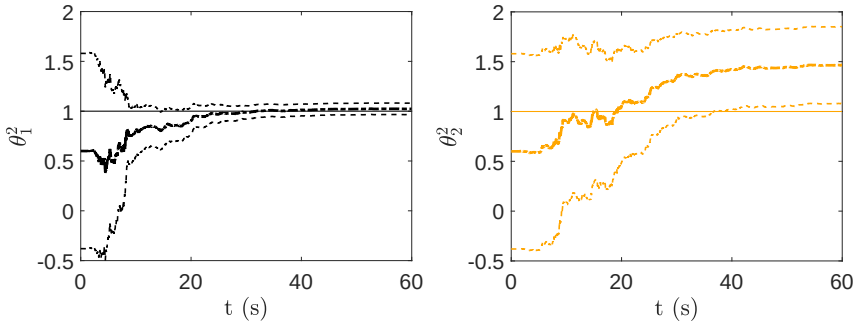

(a) θ_1^2 **(b)** θ_2^2

Figure 5. Model class $\mathcal{M}^2$, time evolution of $\boldsymbol{\theta}^2$. The thicker dotted line reports the posterior estimate, the thinner dotted line the 99% confidence interval of the estimate, determined using the posterior covariance. The continuous line reports the parameter values assumed by the reference model.

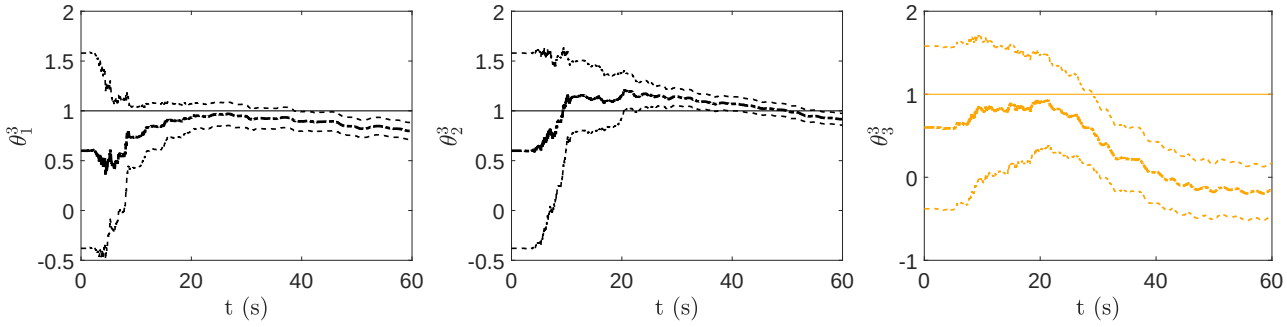

(a) θ_1^3 **(b)** θ_2^3 **(c)** θ_3^3

Figure 6. Model class $\mathcal{M}^3$, time evolution of $\boldsymbol{\theta}^3$. The thicker continuous line reports the posterior estimates, the thinner dotted lines the 99% confidence interval of the estimate, determined using the posterior covariance. The continuous line reports the parameter values assumed by the reference model.

measurements have become available using Eqs. 7 and 8. During the first part of the analysis, $\mathcal{M}^1$ appeared to be the most plausible model class. This is in agreement with intuition: $\mathcal{M}^1$ is the easiest to tune, employing just one parameter, and the bias in the modelling of damping has a marginal relevance when $t < 20$ s due to the strong ground motion undergone by the structure. In a second stage, $\mathcal{M}^3$ resulted to be the most plausible model class. This was due to the good estimate of both the stiffness related parameters and the damping related parameter in the central part of the analysis. Finally, the over complexity of $\mathcal{M}^3$ led to a deterioration of the parameter identification, while the good convergence of the stiffness related parameter and the reasonable damping estimate promoted $\mathcal{M}^2$ as most plausible model class.

This numerical example shows that model evidence evaluation can be successfully used for model selection. The reader should note that, due to the recursive nature of Eq. 7, a certain time delay has occured between the improved identification capacity of the filter equipped with a certain model and the increase in plausibility of this model.

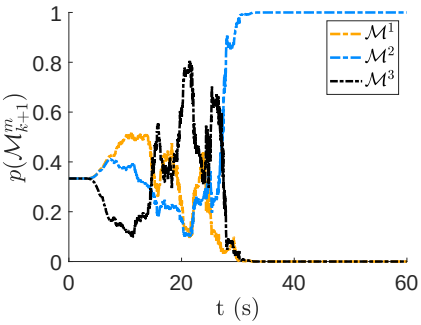

Figure 7. Model evidence evolution of each model.

4. Conclusions

In this work, we have discussed an algorithm for simultaneous parameter estimation and model evidence calculation in dynamic linear elastic problems. Starting from the work of [2], a recursive expression for model evidence evaluation has been derived when the unscented Kalman filter is used. Numerical results show that model evidence can guide system identification in the presence of model uncertainties by associating a plausibility measure to different employed models featuring possible parametrization of the mechanical domain. Indeed, model evidence can be successfully used to select the most plausible structure parametrization as parameter identification is carried out.

Acknowledgments: The authors are indebted to Rodrigo Astroza, Universidad de los Andes (Chile), for the valuable discussions on the topic of this contribution.

References

1. Mariani, S.; Ghisi, A. Unscented Kalman filtering for nonlinear structural dynamics. *Nonlinear Dynamics*, *49*, 131–150. doi:10.1007/s11071-006-9118-9.
2. Yuen, K.V.; Mu, H.Q. Real-time system identification: an algorithm for simultaneous model class selection and parametric identification. *Computer-Aided Civil and Infrastructure Engineering* **2015**, *30*, 785–801. doi:10.1111/mice.12146.
3. Hilber, H.M.; Hughes, T.J.R.; Taylor, R.L. Improved numerical dissipation for time integration algorithms in structural dynamics. *Earthquake Engineering & Structural Dynamics* **1977**, *5*, 283–292. doi:10.1002/eqe.4290050306.
4. Mariani, S.; Corigliano, A. Impact induced composite delamination: state and parameter identification via joint and dual extended Kalman filters. *Computer Methods in Applied Mechanics and Engineering* **2005**, *194*, 5242–5272. doi:10.1016/j.cma.2005.01.007.
5. Eftekhar Azam, S.; Mariani, S.; Attari, N.K.A. Online damage detection via a synergy of proper orthogonal decomposition and recursive Bayesian filters. *Nonlinear Dynamics*, *89*, 1489–1511. doi:10.1007/s11071-017-3530-1.
6. Eftekhar Azam, S.; Mariani, S. Online damage detection in structural systems via dynamic inverse analysis: a recursive Bayesian approach. *Engineering Structures* **2018**, *159*, 28–45. doi:10.1016/j.engstruct.2017.12.031.
7. Gobat, G.; Azam, S.E.; Mariani, S. SHM and efficient strategies for reduced-order modeling. *Engineering Proceedings* **2020**, *2*. doi:10.3390/engproc2020002098.
8. Kopp, R.E.; Orforf, R.J. Linear regression applied to system identification for adaptive control systems. *AIAA Journal* **1963**, *1*, 2300–2306. doi:10.2514/3.2056.
9. Wan, E.; Van Der Merwe, R. The unscented Kalman filter for nonlinear estimation. Proceedings of the IEEE 2000 Adaptive Systems for Signal Processing, Communications, and Control Symposium (Cat. No.00EX373), 2000, pp. 153–158. doi:10.1109/ASSPCC.2000.882463.
10. Julier, S. The scaled unscented transformation. Proceedings of the 2002 American Control Conference (IEEE Cat. No.CH37301), 2002, Vol. 6, pp. 4555–4559 vol.6. doi:10.1109/ACC.2002.1025369.
11. Castiglione, J.; Astroza, R.; Eftekhar Azam, S.; Linzell, D. Auto-regressive model based input and parameter estimation for nonlinear finite element models. *Mechanical Systems and Signal Processing* **2020**, *143*, 106779. doi:10.1016/j.ymssp.2020.106779.
12. D'Alessandro, A.; Vitale, G.; Scudero, S.; D'Anna, R.; Costanza, A.; Fagiolini, A.; Greco, L. Characterization of MEMS accelerometer self-noise by means of PSD and Allan Variance analysis. 7th IEEE International Workshop on Advances in Sensors and Interfaces IWASI, 15-17 June, Vieste, Italy, 2017, pp. 159–164.